Advances in Large Area $Hg_{1-x}Cd_xTe$ Photovoltaic Detectors for Remote Sensing Applications

P.S. Wijewarnasuriya*, M. Zandian, J. Phillips, D. Edwall, R.E. DeWames,
G. Hildebrandt, J. Bajaj and J.M. Arias
Rockwell Scientific, 1049 Camino Dos Rios, Thousand Oaks, CA 91360

A.I. D'Souza
Boeing Sensor Products, 3370 Miraloma Avenue, Anaheim, CA 92803

F. Moore
ITT Aerospace/Communications Division, Ft. Wayne, IN

ABSTRACT

State-of-the-art large area photovoltaic detectors fabricated in HgCdTe grown by Molecular Beam Epitaxy have been demonstrated for the Crosstrack Infrared Sounder (CrIS) instrument. Large area devices (1 mm in diameter) yielded excellent electrical and optical performance operating at 81K for $\lambda_c \sim 15$ μm and at 98K for $\lambda_c \sim 9$ μm and $\lambda_c \sim 5$ μm spectral cut-offs. Fabricated detectors have near-theoretical electrical performance, and AR-coated quantum efficiency is greater than 0.70. Measured average R_oA at 98K is 2.0E7 Ω-cm^2 and near-theoretical quantum efficiencies greater than 0.90 were obtained on detectors with $\lambda_c \sim 5$ μm spectral cut-offs. These state-of-the-art large area photovoltaic detector results reflect high quality HgCdTe grown by Molecular Beam Epitaxy on CdZnTe substrates in all three spectral bands of interested.

Keywords: Molecular Beam Epitaxy (MBE), Remote sensing, HgCdTe, Large area, Photovoltaic detectors, Crosstrack Infrared Sounder

1.0 INTRODUCTION

The demand for larger area photovoltaic detectors that operate in the 5-15 μm spectral wavelength region for remote sensing applications is growing[1-3]. The Crosstrack Infrared Sounder (CrIS) is a key sensor now being developed for the National Polar-orbiting Operational Environmental Satellite System (NPOESS)[4]. CrIS is an interferometric sounding sensor, which accurately measures vertical earth radiances at very high spectral resolution, and uses this data to construct vertical profiles of atmospheric temperature, moisture and pressure. This instrument contains three major spectral bands: namely, SWIR (λ_c ~ 5 μm at 98K), MWIR (λ_c ~ 9 μm at 98K) and LWIR (λ_c ~ 15 μm at 81K) and requires detectors as large as 1 mm in diameter. CrIS Focal Plane Assembly (FPA) consists of 3x3 Focal Plane Arrays[2] each with three spectrally separate SWIR, MWIR and LWIR spectral bands. Traditionally for such applications, photoconductive (PC) detectors have been used. However, photoconductive detectors suffer such serious performance issues[4] nonlinearity in the 1% range, and nonuniform spatial optical response. It is now well-established that PV detectors offer significant advantages over PC for such applications[3].

To address the detector needs of the CrIS instrument, Rockwell Scientific has utilized p-on-n double layer planar heterostructure (DLPH) devices fabricated in molecular beam epitaxy (MBE) HgCdTe grown on lattice matched CdZnTe substrates. Rockwell Scientific has pioneered the development of MBE-grown HgCdTe on lattice-matched CdZnTe (CZT) substrates and device quality MBE material is being grown routinely for applications in the 1-16 μm spectral region[5]. Excellent control of the composition, layer thickness, doping concentration, dislocation density and transport characteristics have been demonstrated[5]. Advances in the MBE growth of HgCdTe and processing capabilities have led to the demonstration of state-of-art detector performance in the entire spectral band discussed above and have resulted in producing high performance large area p-on-n double layer planar heterostructure (DLPH) photovoltaic (PV) detectors. The Tropospheric Emission Spectrometer (TES) is an excellent example of space-borne instrument that utilizes PV MBE-HgCdTe detector arrays[6]. Infrared focal plane array assemblies for the TES consist of four infrared spectral bands (3.3 to 5.3, 5.1 to 9.1, 8.3 to 12.2 and 11.1 to 15.4 μm) with each assembly consisting of a 16-element detector linear array of 75 x 750 μm^2 diodes on a 75 μm pitch. As discussed above, improvements in the material growth, coupled with processing improvements TES, have produced state-of-the-art detectors over a broad spectral range.

This paper describes the performance of 1mm diameter circular (factor of 14 larger than TES detectors) PV detectors covering spectral band λ_c ~ 5 μm to λ_c ~ 15 μm. The paper is structured as follows. Section 2.0 covers MBE HgCdTe material growth/characterization and PV detector fabrication/characterization. Section 3.0 provides Results and section 4.0 summarizes this study.

2.0 HgCdTe MATERIAL GROWTH/CHARACTERIZATION AND PV DETECTOR FABRICATION/CHARACTERIZATION

The detector architecture is based on Rockwell's p-on-n double layer planar heterostructure (DLPH). Benefits of the DLPH architecture[5,7] include a reduction in surface generation-recombination and tunneling currents, and an increase in total dose radiation hardness[8], all of which are essential detector attributes for remote sensing applications. HgCdTe layers were grown by MBE on lattice-matched CdZnTe substrates. The Cd composition and thickness of the grown absorber layer were determined at room temperature by infrared transmission measurements. Hall characteristics (at 2-kG magnetic field strength) of the layers were measured by the van der Pauw technique at 78K.

To characterize the fabricated variable area devices, current vs voltage (I-V) were measured at biases from –200 mV to +200 mV. From these I-V curves, values for dynamic impedance, current density, etc. were calculated. The cut-off wavelength (λ_c) was determined from the point where the spectral response per Watt dropped to 50% of its peak wavelength value (λ_p). The quantum efficiency (QE) was measured with a calibrated blackbody source. A combination of a spot and a flood QE measurement was used to extract the effective lateral optical collection length L_{opt} and hence the optically active area (A_{opt}) of the detectors.

Table I summarizes key flowdown detector parameters required at the operating temperature for each wavelength of the CrIS sensors. Key challenges include:

- Requirement for R_oA near theoretical limited performance, especially on LWIR spectral band and excellent QE (>0.65) on all spectral bands.
- Need larger area (1mm in diameter) detectors; about 18x larger detectors than in the most popular detector format at Rockwell Scientific.
- Larger geometry requires good quality material and hence very low concentration of etch pits (EPD), localized defects.

Due to very stringent CrIS-LWIR detector performance requirements, considerable detector design efforts were concentrated on maximizing CrIS detector performance vs material parameters. Several physical mechanisms are involved in determining dark currents in a photodiode (therefore R_oA). Dark currents can be divided into two mechanisms[9]; thermally generated currents which contribute from the diffusion volume outside the depletion region and currents from depletion/junction origin. Currents from the n-side base region should limit high quality DLPH devices operating in the diffusion-limited region. We have optimized the influence of doping, base layer thickness and cutoff wavelength to the performance of an abrupt p+-n photodetectors using classical one-dimensional model discussed in the literature[10]. The R_oA product and QE (η) were taken as the figure of merit in order to maximize the CrIS detector performance vs material parameters. The thickness of the base n-

type layer was optimized for quantum efficiency and for low dark current. In all three cases base layer thickness greater than the inverse absorption coefficient at the peak wavelength was selected.

For larger area detectors, the yield and performance of HgCdTe devices are limited primarily by extended defects such as dislocations, voids, and inclusions. Hence, the presence of growth-induced voids and etch pit clusters will be detrimental to large area HgCdTe PV devices; a one-to-one correlation between the presence of these "killer" defects within the active area and poor device performance has been reported[11]. The density of void defects must be as low as possible since these defects are device "killers". Measured EPD on the wafers discussed in this paper is in the low10^4 cm^{-2} levels and void density is less than mid 10^3 levels. N-type active layer was doped in situ during MBE growth with indium in high 10^{14} cm^{-3} to low 10^{15} cm^{-3} levels.

3.0 RESULTS AND DISCUSSION

Detector Performance

Spectral response vs wavelength was measured on all of the detectors under backside illuminated condition. Measured peak wavelength (λ_p), cutoff wavelength (λ_c), QE (η) and minority carrier optical length (L_{opt}) are listed in Table II. Measured average λ_p on SWIR devices is 4.56 μm and average cutoff λ_c is 5.01 μm, which is about 10% longer than λ_p. On MWIR devices, measured average λ_p is 8.00 μm and average cutoff λ_c is 9.07 μm, which is about 13% longer than λ_p. On LWIR devices, measured average λ_p is 13.33 μm and average cutoff λ_c is 15.29 μm, which is about 15% longer than λ_p. For both SWIR and MWIR spectral curves, fall-offs are sharp; and LWIR curves, fall-off is slightly soft and may be due to relatively thin 13 micron base layer thickness (see Fig.1c). Measured average L_{opt} from optical measurements on devices with cutoff at 98K ~ 5 micron is 43 microns; which is in good agreement with the defect-free 1-D theory in the absence of recombining interfaces. Measured average L_{opt} on devices with cutoff at 98K ~9 micron is 29 microns and with cutoff at 81K ~15 micron is 15 microns. Representative spectral response per photons as a function of wavelength is displayed in Fig. 1 for the three spectrally separate SWIR, MWIR and LWIR detectors. Detectors are AR-coated to reduce the reflection losses due to CZT back interface. The reflection loss from the back CZT interface is 21% and with AR coating QE is enhanced approximately by this value. Figure 1 shows that, in all cases flat spectral QE was measured in each spectral band. Observed dip(s) at ~ 4.2 μm and ~ 5.5 to 6.2 μm wavelengths are due to atmospheric absorption bands due to CO_2 absorption and is an artifact due to the measurement system.

The measured quantum efficiency on SWIR devices is greater than 0.90 (greater than 0.72 is required), which is closer to the expected value using device parameters. In MWIR detectors measured quantum efficiency is 0.80 (greater than 0.72 is required) in the 5.92 μm to 8.00 μm spectral band, dropping off in the 8.00 μm to 8.26 μm portion of the spectral band. In both cases measured QE is bias-independent at reverse bias, which indicates no valence band barriers/series resistance issues.

High-quality DLPH devices operating in the diffusion limited region should be limited by currents from the n-side with the active (absorber) layer thickness d less than the diffusion length. If these conditions are met, the current-voltage relationship for PV detectors can be expressed as[11];

$$I = \frac{qn_i^2 d}{N_d \tau_p}\left(\exp\left(\frac{qV_d}{nkT}\right)-1\right)$$

where q is the electron charge, k is Boltzmann's constant, T is absolute temperature, n is an empirical slope factor ~ 1-2, V_d is the bias voltage across the diode, n_i is the intrinsic concentration, N_d is the base layer donor concentration, d is the base layer thickness, and τ_p is the material radiative and Auger lifetime. Ideally, n = 1 for diffusion current component and 2 for generation-recombination component[12].

Figure 2 displays representative I_d-V_d and R_dA versus voltage curves for a 4.97 μm cutoff detector operating at 98K. Area of the device is $7.85x10^{-3}$ cm^2. The R_oA value is $6.2x10^7$ ohm-cm^2 at 98K. For the detector displayed in Figure 2, the dark current is $6x10^{-12}$ amps at –100 mV and R_dA maximum is $1.0x10^9$ ohm-cm^2 at 70 mV reverse bias. Measured I-V data can be fitted with diode equation as described above, assuming defect-free material lifetime. The solid line in the figure is the theoretical diffusion curve calculated from the measured material parameters. The theory is based on a simple one-dimensional model which assumes diffusion currents from the n-type side. Also Fig. 2 displays dynamic impedance times area product (R_dA) vs voltage. The detector is diffusion limited near zero bias and the dynamic impedance peaks at –70 mV reverse bias. At reverse bias voltages down to –200 mV show no sign of tunneling currents. Instead, some sort of shunt current dominates, possibly due to the instrumentation. Very good agreement between the measured dark current near zero bias and calculated values is seen. Dashed line in the figure is the diffusion slope with ideality factor equals to 1.13 indicating near diffusion limited performance.

Figure 3 display R_oA product and QE vs cut-off wavelength on SWIR devices from wafer 2-1206. Measured R_oA (where A= 7.85E-3 cm^2) is an order of magnitude higher than the flow-down specification. The ratio between R_dA (at –100mV) to R_oA is about 5.

Figure 4 displays measured dark current and dynamic impedance-area product (R_dA) versus bias voltage (V_d) curves for LW at 81K measured on a CrIS detector from wafer 3-288. The R_dA versus V_d curve shows that the series and contact resistances are comparable to the junction impedance at zero bias. When the detector is held at zero bias, the quantum efficiency cannot be extracted due to high pre-amplifier noise induced by a low detector impedance. Severely depressed QE at zero bias was obtained in all of the LWIR devices. At reverse bias of –100mV the measured ~ 0.70 (in some cases 0.85) quantum efficiencies (greater than 0.60 is required). Therefore, the detector needs to be operated in reverse bias where the junction impedance is significantly higher than the series/contact resistance. Measured R_dA ~ 10^2 ohm-cm^2 range at –100mV reverse bias. This is about two orders of magnitude

higher than impedance-times-area product (R_oA) at zero bias, and indicates excellent quality larger area LWIR PV devices.

The solid line in Fig. 4 is the theoretical diffusion current assuming from n-side only. Measured cutoff is 15.1 microns at 81K. The model uses measured material parameters, such as carrier concentration, active layer thickness and measured λ_c as described before. The Cd composition is obtained from the spectral response vs wavelength fit at 81K. Fig. 4 shows that measured dark current agrees very well with the calculated dark currents down the ~ 75 mV reverse bias, indicating dominant currents are diffusion origin. I_d-V_d versus voltage curve illustrates that diffusion current from n-side dominates over a considerable large region of reverse bias voltage. The dashed line in the figure with n ~1.3 further confirms these currents. A slightly higher n value is probably due to the current contribution close to zero bias from the series/contact resistance effects. At high reverse bias voltages tunneling takes over. Since the LW detectors is to be operated in reverse bias, the dark current in reverse bias is the important performance parameter rather than the R_oA value. For detectors displayed in Table II, measured dark current at –100 mV ranges from 43 μA to 79 μA at 81K, which is factor of two below specification for LW band (see Table I). Also, spatial cutoff uniformity is a key factor in LWIR (λ_c ~ 15 μm), especially in very large area detectors. From Table II, measured average cutoff wavelength λ_c yielded 15.3 μm with a standard deviation of 0.13 μm across 4 x 4 cm^2 wafer, indicating very uniform 15 μm wavelength MBE material on larger area wafers.

Figure 5 displays representative I_d-V_d and R_dA versus voltage curves for a 8.97 μm cutoff detector operating at 98K. Area of the device is 7.85×10^{-3} cm^2. The R_oA value is 6.2×10^7 ohm-cm^2 at 98K. Very good agreement between the measured R_dA and calculated values down to -50 mV reverse bias voltages indicates dominant currents are from n-side diffusion. Figures 6 display R_oA, R_dA (at –100mV) products and QE vs wavelength on MWIR devices. Measured R_oA on MWIR devices from wafer 2-1241 is twice the required value (R_oA greater than 50 is required). R_dA at –100mV is in the 1E4 Ω-cm^2. Measured average R_oA of detectors from wafer 2-1241 is 130 Ω-cm^2 at 98K which is near-theoretical. Impedance times area product peaks at ~70mV reverse bias. Similar to the LWIR devices, diffusion currents dominate near zero bias down to ~ 70 mV of reverse bias. Measured cutoff wavelength ranges from 8.87 μm to 9.11 μm at 98K from wafer 2-1241. Nevertheless, in all three cases these measured high L_{opt} and R_oA reflect the base material quality and further confirm measured high η.

4.0 Summary

Excellent device quality MBE-HgCdTe material has been grown for the Crosstrack Infrared Sounder (CrIS) instrument. This is a key sensor(s) now being developed for the National Polar-orbiting Operational Environmental Satellite System (NPOESS). Fabricated large area devices (1 mm in diameter) demonstrated excellent electrical and optical device performance operating at 81K for LWIR band and for 98K for MW and SWIR bands. LWIR and MWIR detectors have near theoretical electrical performance. AR-coated quantum efficiency in LWIR detectors is greater than 70%. In MWIR detectors measured quantum efficiency is 0.80 in the 5.92 μm to 8.00 μm spectral band, dropping off in the 8.00 μm to 8.26 μm portion of the spectral band. Performance in SWIR detectors shows an order of magnitude higher than the flow-down requirements, and near theoretical quantum efficiencies in the 90% range were obtained. In all three cases, excellent spectral uniformity was obtained across larger area wafers grown by MBE.

5.0 ACKNOWLEDGMENTS

This work was supported by the Boeing Company under the contract number A9HG-568018-F-809.

6.0 REFERENCES

1. E.E. Krueger, D. Lee, C. Miller, C.L. Terzis, P.O'Dette, B. Denley, J. Rutter, J.L. Williams and M.B. Reine, Proc. Of SPIE **Vol. 3122**, Infrared Spaceborne Remote Sensing V (Oct. 1997).
2. A.I. D'Souza, L.C. Dawson, S. Marsh, R. Willis , P.S. Wijewarnasuriya, R.E. DeWames, J. M. Arias, J. Bajaj, G. Hildebrandt and F. Moore, SPIE 2001.
3. M.B. Reine, Proc. SPIE 2001.
4. R. J. Glumb, D. C. Jordan, and J. P. Predina, SPIE 2000.
5. J. Bajaj, Proc. SPIE 3948 (2000).
6. C.F. Bruce, J. Bjaj, D. Lee, T.A. Pepper, G. Chu, W.V. McLevige, D.D. Edwall, L.A. McGregor, W. Weissbard, G. Hildebrandt, J.D. Blackwell, S. Bhargava, V. Gil, D.E. Cooper, K. Spariosu, J.M. Arias, W.E. Tennant, K. Vural and L. Shin, "Infrared Detector Assemblies for the Tropospheric Emission Spectrometer," Proc. IEEE Aerospace Conf., March 18-25, Big Sky, Montana (2000).
7. A.I. D'Souza, L.C. Dawson, E.J. Anderson, A.D. Markum, W.E. Tennant, L.O. Bubulac, M. Zandian, J.G. Pasko, W.V. McLevige, D.D. Edwall, *J. Electron. Mater.* **26**, 656 (1997).
8. J.M. Arias, J.G. Pasko, M. Zandian, S.H. Shin, G. M. Williams, L.O. Bubulac, R.E. DeWames, W.E. Tennant, *Appl. Phys. Lett*. **62**, 976 (1993).
9. M.B. Reine, T.J. Tredwell, A.K. Sood, "Photovoltaic Infrared Detectors" chapter, Semiconductors and Semimetals **Vol. 18**, R.K. Willardson and A.C. Beer editors, Academic Press, NY, 1981.
10. G.M. Williams, R.E. DeWames, *J. Electron. Mater.* **24**, 1239 (1995).

11. P.S. Wijewarnasuriya, M. Zandian, D.B. Young, J. Waldrop, D.D. Edwall, W. V. McLevige, D. Lee, J. Arias and A.I. D'Souza, J. of Elect. Mater. **28**, 649 (1999)
12. J.P. Mckelvey, Solid State and Semiconductor Physics, Harper and Row, NY, 1966, p.422
13. A. Rogaliski and J. Piotrowski, Prog. Quantum Electronics, **12**, 87 (1988)

* Author Contact Information: Tel. (805)-373-4626, FAX: (805)-373-4137, e-mail: WIJE@RWSC.COM

Table I. CrIS flow down detector performance parameters

Parameter	**Units**	**SWIR**	**MWIR**	**LWIR**
Detector Architecture		p-on-n	p-on-n	p-on-n
Detector Diameter	μm	1000	1000	1000
Cutoff wavelength	μm	5.0	8.9	15.3
Operating Temp	K	98	98	81
Spectral Band	μm	3.92 - 4.64	5.71 - 8.26	9.13 - 15.38
AR-coated QE		> 0.75	> 0.72	> 0.60
R_oA	Ω-cm^2	**> 6.0E5**	**> 50**	**> 0.75**
Dark Current at -100mV	Amps	< 1.7E-10	< 2.0E-6	< 1.35E-4

Table II Summary of measured device characteristics. Area of device is 7.85E-3 cm^2.

Wafer #	Diode #	L_{opt} (μm)	Spectral Response λ_p (μm)	Spectral Response λ_c (μm)	Spectral Response $\Delta\lambda/\lambda p$	QE (AR Coated)	R_oA ohm-cm^2	R_dA ohm-cm^2 at -0.1V	I_d Amps at -0.1V
						at 98K			
						at 4 μm			
	12,9		4.51	4.97	10%	--	4.26E+07	8.72E+08	7.11E-12
	12,6		4.56	4.98	9%	0.91	1.17E+07	1.45E+08	1.14E-11
	11,2		4.57	5.00	9%	--	2.85E+07	1.36E+08	1.09E-11
	11,9		4.60	5.00	9%	0.95	2.11E+07	1.83E+08	9.28E-12
2-1206	2,2	43	4.52	5.00	11%	0.88	4.70E+07	1.13E+08	9.93E-12
	3,5		4.60	5.02	9%	--	7.81E+06	9.80E+06	5.36E-11
	4,10		--	5.02	--	0.94	5.70E+06	1.04E+07	5.10E-11
	5,2		4.62	5.02	9%	0.94	2.09E+07	4.40E+07	1.50E-11
	1,3		4.48	5.02	12%	0.88	2.95E+07	1.05E+08	8.88E-12
	6,2		--	5.04	--	0.95	5.41E+06	3.44E+07	3.49E-11
						at 98K			
						at 8.3 μm			
	12_2		7.89	8.97	14%	0.70	1.84E+02	1.30E+04	3.58E-07
	7_1		8.00	8.99	12%	0.67	1.32E+02	4.03E+03	6.74E-07
	5_10		7.98	9.01	13%	0.71	1.46E+02	7.81E+03	5.07E-07
	10_2		7.97	9.05	14%	0.71	1.45E+02	1.11E+04	4.83E-07
	4_3		8.02	9.06	13%	0.70	1.28E+02	4.03E+03	6.57E-07
	5_3		8.11	9.07	12%	0.71	1.35E+02	6.20E+03	6.20E-07
2-1241	11_6	29	7.98	9.08	14%	0.72	1.32E+02	1.59E+04	4.86E-07
	6_3		7.98	9.08	14%	0.72	1.18E+02	5.35E+03	7.14E-07
	9_7		7.98	9.10	14%	0.72	1.25E+02	4.82E+03	6.59E-07
	7_5		8.05	9.10	13%	0.72	1.12E+02	6.74E+03	6.96E-07
	6_4		--	9.10	--	0.67	9.71E+01	2.94E+03	9.86E-07
	8_4		8.03	9.10	13%	0.70	1.23E+02	6.30E+03	6.24E-07
	8_6		7.93	9.11	15%	0.71	1.26E+02	1.06E+04	5.40E-07
	9_4		8.03	9.11	13%	0.72	1.16E+02	6.56E+03	6.11E-07
						at 81K			
						at 9.00 μm			
	12_2		13.4	15.1	13%	0.75	1.57	1.30E+02	4.37E-05
	7_5		13.5	15.2	13%	0.73	1.47	1.45E+02	6.56E-05
	12_6		--	15.2	--	0.70	1.31	8.68E+01	5.86E-05
	10_5		13.1	15.2	16%	0.71	1.17	1.56E+02	5.99E-05
	8_10		13.4	15.2	13%	0.70	1.68	8.13E+01	6.05E-05
	8_1		13.2	15.3	16%	0.73	1.47	1.18E+02	4.84E-05
3-288	8_7	15	13.3	15.3	15%	0.73	1.52	1.40E+02	6.06E-05
	10_2		13.2	15.3	16%	--	1.79	7.10E+01	5.16E-05
	3_8		13.2	15.3	16%	0.73	1.92	1.45E+02	4.28E-05
	6_7		13.4	15.4	15%	0.72	1.69	4.71E+01	7.13E-05
	7_1		13.4	15.4	15%	0.72	1.65	1.51E+02	5.41E-05
	5_4		13.5	15.6	16%	0.73	1.16	5.21E+01	7.86E-05

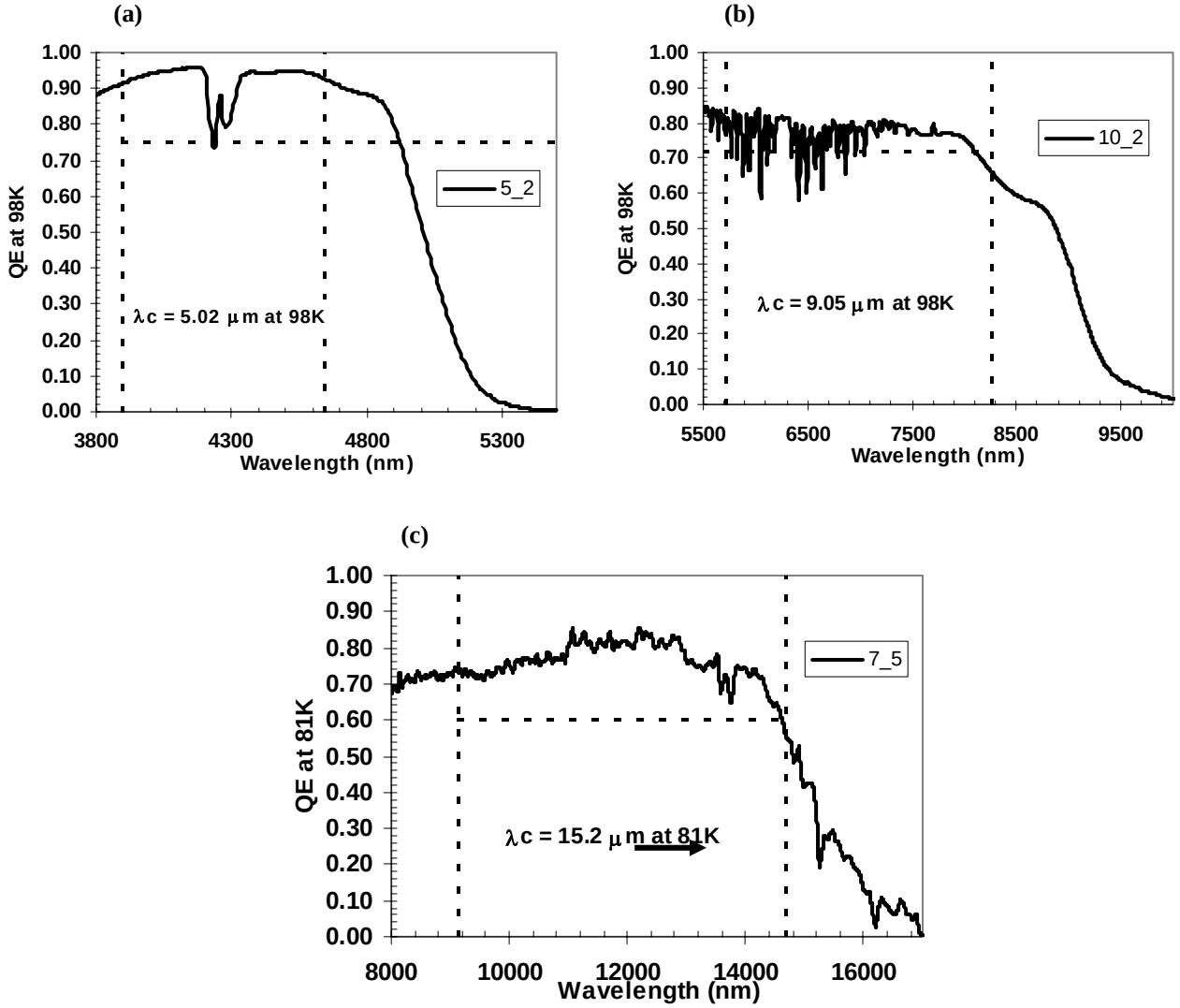

Fig. 1 Absolute spectral response curves for (a) SWIR at 98K for device 5_2 (b) MWIR at 98K for device 10_2and (c) LWIR at 81K for device 7_5 on 1mm diameter MBE p-on-n HgCdTe PV-detectors. Dashed lines are the required QE specification of the CrIS program.

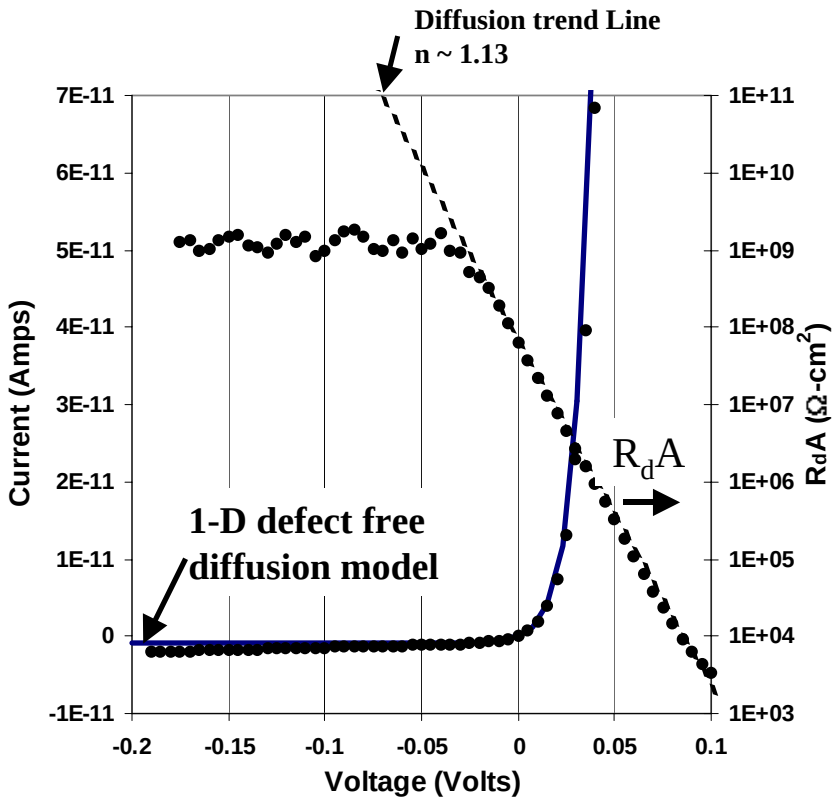

Fig. 2 Current-Voltage and R_dA product (where A= 7.85E-3 cm^2) curves for photodiode # 5_2 from wafer 2-1206. Measured cutoff is 4.97 μm at 98K. The dashed line shows the diffusion trend line which follows measured data down to ~ 50 mV and the solid line shows the 1-D model discussed in the text.

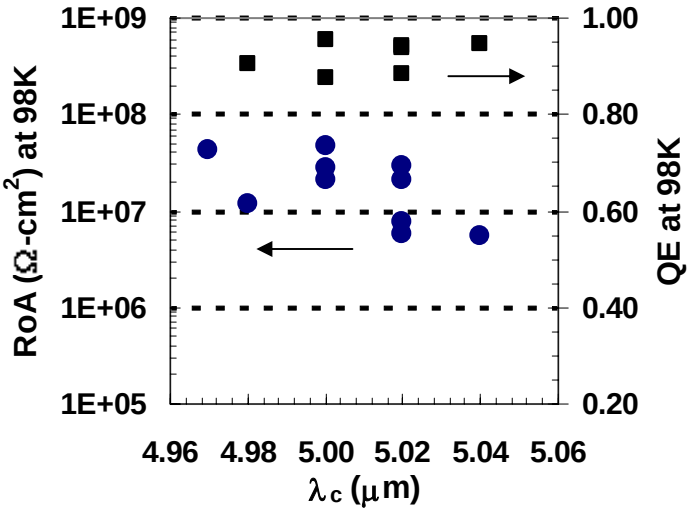

Fig. 3 Measured dynamic impedance-times-area product and QE vs cutoff wavelength at 98K on CrIS SWIR detectors from wafer #2-1206. Measured average cutoff at 98K is 5.01 μm and area of the device is 7.85E-3 cm^2.

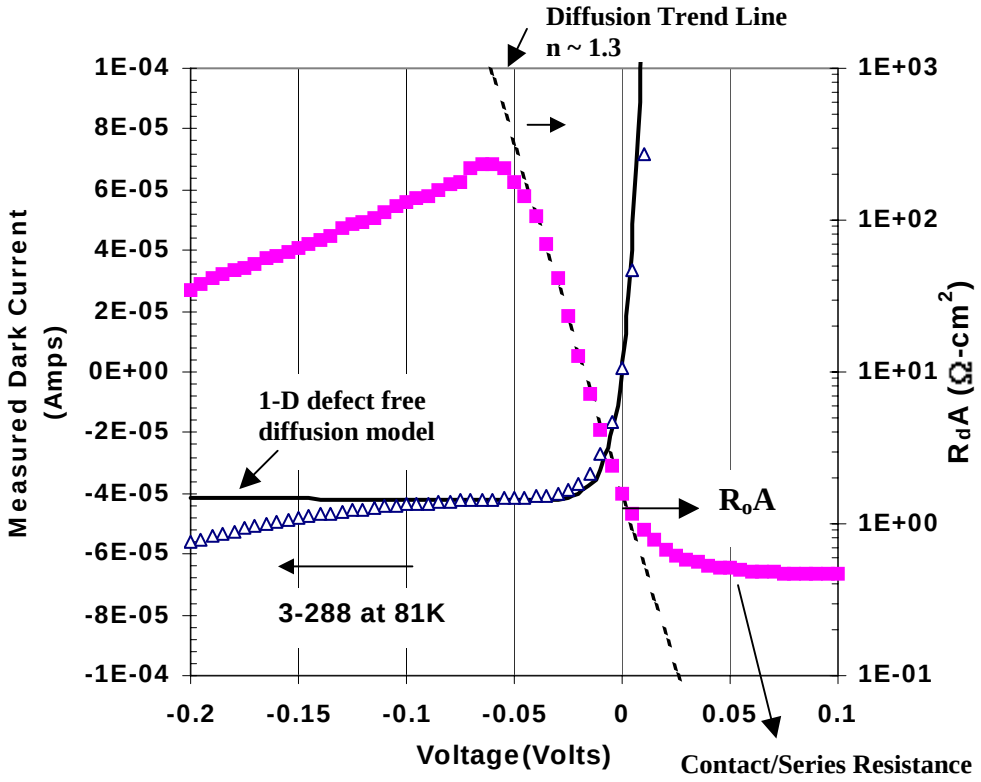

Fig. 4 Current-Voltage and R_dA product (where A= 7.85E-3 cm^2) curves for photodiode # 12_2 from wafer 3-288. Measured cutoff is 15.1 μm at 81K. The dashed line shows the diffusion trend line which follows measured data down to ~ 50 mV and the solid line shows the 1-D model discussed in the text.

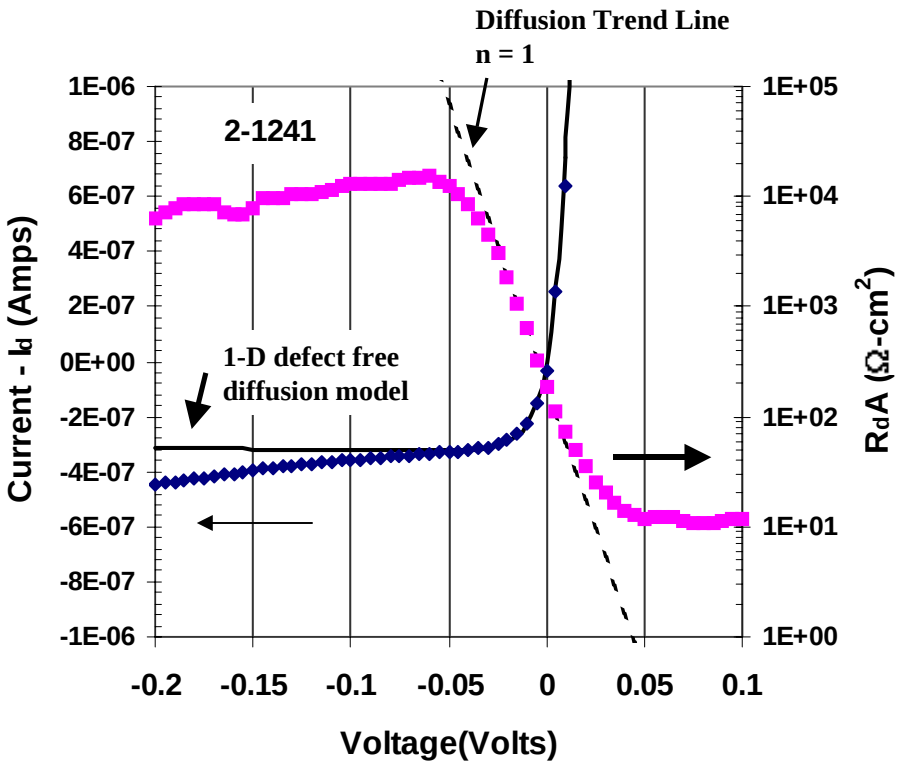

Fig. 5 Current-Voltage and R_dA product (where A= 7.85E-3 cm^2) curves for photodiode # 12_2 from wafer 2-1241. Measured cutoff is 8.97 μm at 98K. The dashed line shows the diffusion trend line which follows measured data down to ~ 50 mV and the solid line shows the 1-D model discussed in the text.

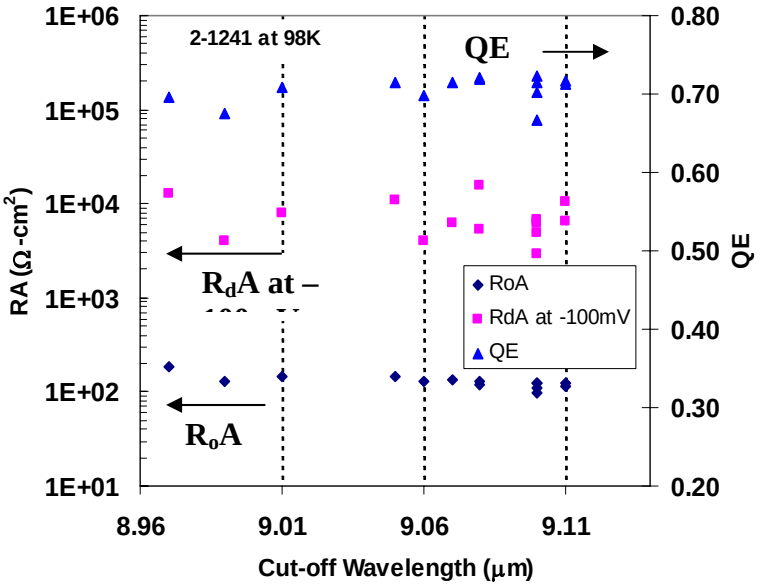

Fig. 6 Measured dynamic impedance-times-area product and QE vs cutoff wavelength at 98K on CrIS MWIR detectors from wafer #2-1241. Measured average cutoff at 98K is 9.07 μm and area of the device is 7.85E-3 cm^2.